Structures of Langya Virus Fusion Protein Ectodomain in Pre- and Postfusion Conformation

Aaron J. May,[a,b] Karunakar Reddy Pothula,[a] Katarzyna Janowska,[a] Priyamvada Acharya[a,b,c]

aDuke Human Vaccine Institute, Durham, North Carolina, USA
bDuke University, Department of Biochemistry, Durham, North Carolina, USA
cDuke University, Department of Surgery, Durham, North Carolina, USA

ABSTRACT Langya virus (LayV) is a paramyxovirus in the *Henipavirus* genus, closely related to the deadly Nipah (NiV) and Hendra (HeV) viruses, that was identified in August 2022 through disease surveillance following animal exposure in eastern China. Paramyxoviruses present two glycoproteins on their surface, known as attachment and fusion proteins, that mediate entry into cells and constitute the primary antigenic targets for immune response. Here, we determine cryo-electron microscopy (cryo-EM) structures of the uncleaved LayV fusion protein (F) ectodomain in pre- and postfusion conformations. The LayV-F protein exhibits pre- and postfusion architectures that, despite being highly conserved across paramyxoviruses, show differences in their surface properties, in particular at the apex of the prefusion trimer, that may contribute to antigenic variability. While dramatic conformational changes were visualized between the pre- and postfusion forms of the LayV-F protein, several domains remained invariant, held together by highly conserved disulfides. The LayV-F fusion peptide (FP) is buried within a highly conserved, hydrophobic interprotomer pocket in the prefusion state and is notably less flexible than the rest of the protein, highlighting its "spring-loaded" state and suggesting that the mechanism of pre-to-post transition must involve perturbations to the pocket and release of the fusion peptide. Together, these results offer a structural basis for how the Langya virus fusion protein compares to its Henipavirus relatives and propose a mechanism for the initial step of pre- to postfusion conversion that may apply more broadly to paramyxoviruses.

IMPORTANCE The *Henipavirus* genus is quickly expanding into new animal hosts and geographic locations. This study compares the structure and antigenicity of the Langya virus fusion protein to other henipaviruses, which have important vaccine and therapeutic development implications. Furthermore, the study proposes a new mechanism to explain the early steps of the fusion initiation process that can be more broadly applied to the *Paramyxoviridae* family.

KEYWORDS conformational change, fusion peptide, fusion protein, glycoprotein, henipavirus, paramyxovirus, viral entry, viral protein, cryo-EM, structural biology

Langya virus (LayV) is a newly identified member of the *Henipavirus* genus, detected after surveillance of disease following animal exposure in eastern China (1). Over the course of several years, LayV infections were identified in 35 individuals, 26 of whom were infected solely with LayV. In these 26 individuals, common symptoms included fever, fatigue, cough, nausea, and headaches. The genome organization of LayV is identical to that of other henipaviruses, including the better-known and highly virulent Nipah (NiV) and Hendra (HeV) viruses. Based on phylogenetic analysis, LayV is most closely related to Mojiang virus (MojV), which was discovered in rats in southern China (2), and Gamak (GAKV) and Daeryong (DARV) viruses, which were detected in shrews in the Republic of Korea (3).

The henipaviruses infect a range of animals, with Nipah and Hendra viruses having their natural reservoir in fruit bats (4). However, several additional *Henipavirus* species have been discovered in recent years with differing animal reservoirs. A survey of both domestic and wild animals revealed a low level of seropositivity for LayV in goats and dogs (2% and 5%, respectively) and the highest positivity rate (52.1%) in shrews (*Crocidura lasiura* specifically), indicating that shrews may be the natural reservoir for LayV. The *Henipavirus* genus is a member of the *Paramyxoviridae* family (5), which includes both extremely infectious human pathogens, such as measles and mumps, and extremely deadly pathogens, such as Nipah and Hendra. This diversity of infectivity and virulence, as well as diversity of animal reservoirs, are risk factors that necessitate paramyxovirus research. Accordingly, Nipah and Hendra viruses are listed as priority pathogens by the WHO (6).

Henipaviruses present two surface glycoproteins known as the attachment and fusion proteins. These proteins work together to mediate viral entry into host cells, and in Nipah virus, both have been shown to be required for viral entry (7). As these are the sole virus surface-expressed proteins, they are also the primary targets of neutralizing antibodies against henipaviruses. The *Henipavirus* attachment protein has receptor-binding capability and, in Nipah and Hendra viruses, binds to ephrin B2 and B3, which are found mostly in the brain and endothelial cells in the heart and lungs (8, 9). The *Henipavirus* fusion (F) protein is a class I fusion protein that has a metastable prefusion conformation, which is displayed on virion surfaces prior to receptor engagement, and a postfusion conformation that is adopted after virus-cell fusion (10, 11). Proteolytic cleavage splits F into two subunits, F_1 and F_2, still connected by disulfide linkages (10, 12), freeing a series of hydrophobic residues known as the fusion peptide (FP) to be inserted into the host cell membrane during this conformational conversion. This process anchors the virus to the host cell and allows the formation of a six-helix bundle in the F protein to bring the viral and host membranes together, facilitating fusion. Although it has many mechanistic features in common with other class I fusion proteins, the F protein in paramyxoviruses does not appear to have any primary receptor-binding functionality. This role is fulfilled by a separate attachment glycoprotein, which is believed to undergo conformational changes during receptor binding, which pass a triggering signal to F (13, 14). The structural basis for this process is poorly understood.

Here, we determine cryo-electron microscopy (cryo-EM) structures of the LayV fusion protein (LayV-F) in pre- and postfusion conformations, both at 4.64 Å resolution, with both structures obtained from the same cryo-EM data set. The LayV-F ectodomain sequence as reported by Zhang et al. was used (1) (Fig. S1), replacing the transmembrane and cytoplasmic domains with purification tags and a trimerization domain. No prefusion stabilizing mutations were made, nor was the fusion protein cleaved or otherwise knowingly induced to convert to the postfusion state. Therefore, the presence of both conformations suggests that the protein was in a state of spontaneous conversion during vitrification. We compare it to other known *Henipavirus* fusion protein structures and elucidate the structural basis for pre- to postfusion conversion in both LayV and more broadly for *Henipavirus* fusion proteins. Our study demonstrates that the highly conserved paramyxovirus fusion protein architecture is utilized by LayV-F, identifies a region of variability among *Henipavirus* fusion proteins in an important antigenic site, and provides evidence for a mechanism to describe how *Henipavirus* fusion proteins are triggered to undergo conformational changes during the fusion process.

RESULTS

Purification and structural determination of LayV-F. We purified the LayV-F ectodomain based on protocols previously developed for NiV-F by expressing in 293F cells and purifying via Strep-Tactin (IBA Lifesciences) affinity chromatography followed by size exclusion chromatography (SEC) (Fig. S2). Like the NiV-F protein, the LayV-F ectodomain elutes with a distinct peak at ~180 kDa. Higher-molecular-weight species, broader than the main peak, were also observed at ~400 kDa and above (see Fig. S2A in the supplemental material). These could be the result of low-affinity interactions between individual trimers. SDS-PAGE analysis of these high-molecular-weight species in both NiV-F and LayV-F purifications has consistently produced identical bands corresponding to the

~180-kDa species, consistent with the uncleaved F protein (Fig. S2E). Higher-order multimers of henipavirus F proteins with rings described as "hexamers of trimers" have been previously reported (15). While larger-molecular-weight species were detected during purification of LayV-F (Fig. S2A), they comprised a far lower proportion of total protein than purifications of wild-type NiV-F and a prefusion-stabilized NiV-F mutant, NiVop08 (Fig. S2A) (16). The yield of LayV-F at ~1.2 mg/L was considerably higher than that of wild-type NiV-F at ~250 μg/L. The NiVop08 yield was vastly higher than the unstabilized NiV-F construct at ~3 mg/L, consistent with the general trend of prefusion-stabilized fusion protein constructs expressing more efficiently than their wild-type counterparts (17–20). Differential scanning fluorimetry (DSF) suggested reduced stability of LayV-F compared to NiV-F (Fig. S2B). The LayV-F DSF profile closely resembles that of wild-type NiV-F but is left shifted, indicating that the temperature-induced conformational changes or unfolding events are occurring at a lower temperature for LayV-F.

We determined the structure of the LayV-F ectodomain trimer using cryo-EM. Reference-free two-dimensional (2D) classes revealed both pre- and postfusion conformations of LayV-F in the cryo-EM data set (Fig. 1A and B). After several rounds of classification and sorting, we obtained 4.64-Å reconstructions (calculated within cryoSPARC according to the Fourier shell correlation [FSC] 0.143 gold-standard criterion) of the prefusion and postfusion forms of the LayV-F protein from approximately 200,000 and 80,000 particles, respectively. Assessment of the three-dimensional FSC (3DFSC) plot for these maps indicated resolutions of 5.42 Å and 5.25 Å for the pre- and postfusion conformations, respectively (21). The structures determined revealed pre- and postfusion architectures that were similar to those determined for other paramyxoviruses (15, 22–26). The prefusion LayV-F structure has a compact "clove-like" shape with a large internal cavity and spans ~110 Å from the bottom of the stalk to the top of the apex. In comparison, the postfusion structure is elongated, spanning ~160 Å, with regions that formed the prefusion apex straightening into a central coiled-coil, ending with the trademark six-helix bundle of the postfusion conformation.

The LayV-F ectodomain includes a fusion peptide (FP) and two heptad repeat sequences that both contribute to three domains, previously described by Yin et al. for the parainfluenzavirus 5 (PIV5) F protein (Fig. 1C to E) (26). Domain I (DI) is comprised of the most N-terminal residues after cleavage of the signal peptide, 22 to 45, and residues 278 to 369. Its central β-sheet connects domain II (DII) to the apical domain III (DIII). DII, from residues 370 to 446, makes significant contact with the cleavage site and fusion peptide of the neighboring protomer before leading to heptad repeat B (HRB), located at the most C-terminal end of the ectodomain. DIII, from residues 46 to 277, contains the cleavage site, fusion peptide, and heptad repeat A (HRA) (Fig. 1C to E). Residues 93 to 140 from DIII and 441 to 450 from DII, which become linker regions leading to the repositioned heptad repeats now forming the six-helix bundle, are not resolved in the postfusion structure (Fig. 1E).

Pre- to postfusion conversion mechanism of LayV-F. Though the *Henipavirus* genus was established with the discovery of Hendra virus in 1994 (4, 27), the number of members of the genus has dramatically expanded in recent years with the discovery not only of Langya virus but also Gamak and Daeryong viruses, both identified in 2021 (3). Within the past 3 years, henipaviruses have been identified in an expanded range of animal hosts and geographic locations. No longer contained in southeast Asia and Australia, new species have been discovered in Africa and South America, specifically Angavokely virus and Peixe-Boi virus, respectively (28, 29). Although there is very high structural similarity for fusion proteins across not only the *Henipavirus* genus but within the larger *Paramyxoviridae* family, there tends to be low sequence identity between species, with LayV-F having ~40% sequence identity with NiV-F and ~30% or less identity to other non-*Henipavirus* paramyxoviruses (Fig. S1). However, with more *Henipavirus* members identified, some conserved sequence features have become more evident. These include 10 highly conserved cysteines present in the ectodomain of paramyxovirus F proteins (Fig. 2). Identifying the locations of these cysteines in the pre- and postfusion LayV-F structures reveals their critical role in maintaining domain fold integrity during the dramatic conformational changes that occur during fusion.
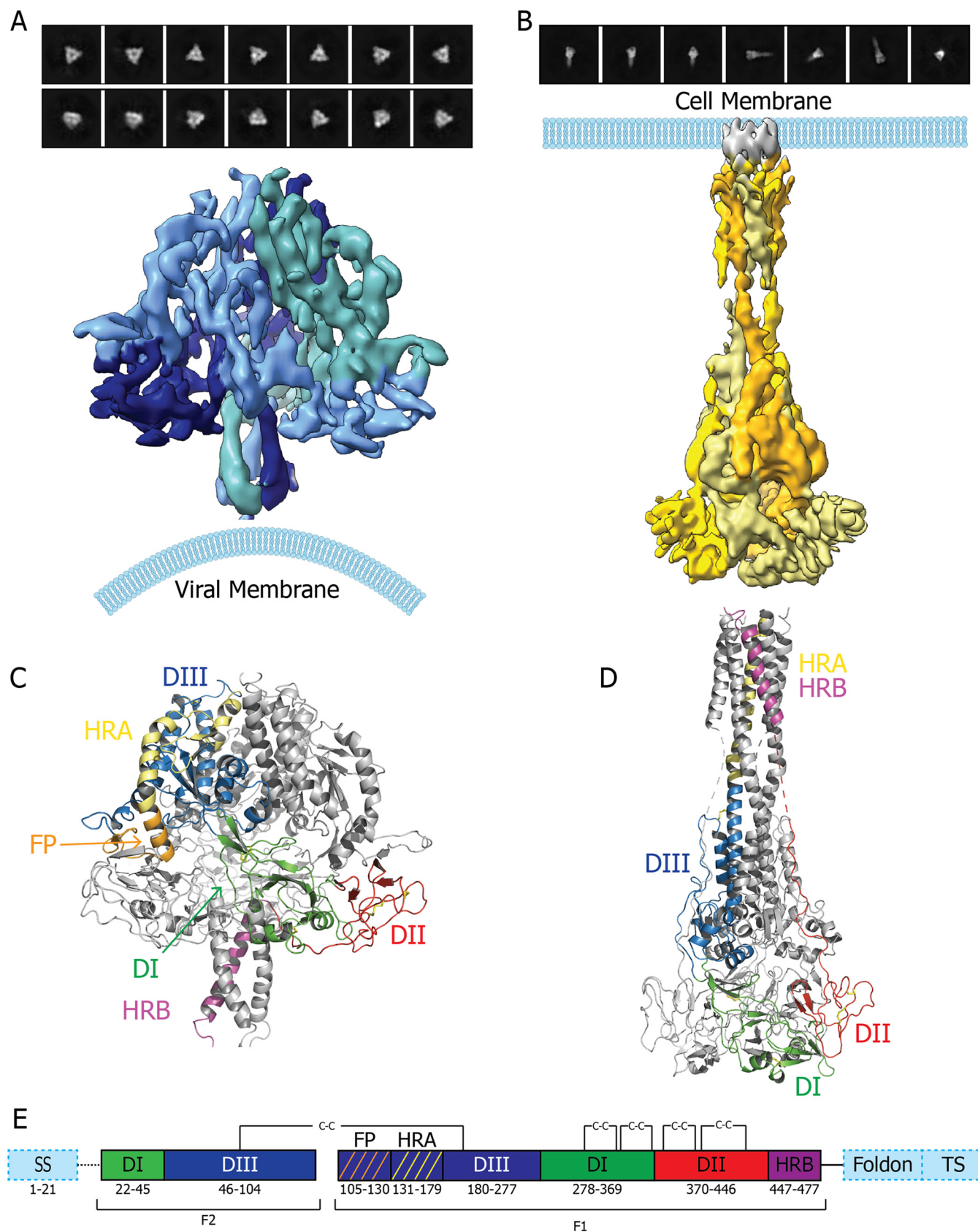
FIG 1 Structures of LayV-F in pre- and postfusion conformation. Cryo-EM maps of the pre- and postfusion conformations of LayV-F along with the fitted models with a sequence key. (A and B) Cryo-EM reconstructions of LayV-F in prefusion (A) and postfusion (B) conformations, colored by protomer. Map regions colored in
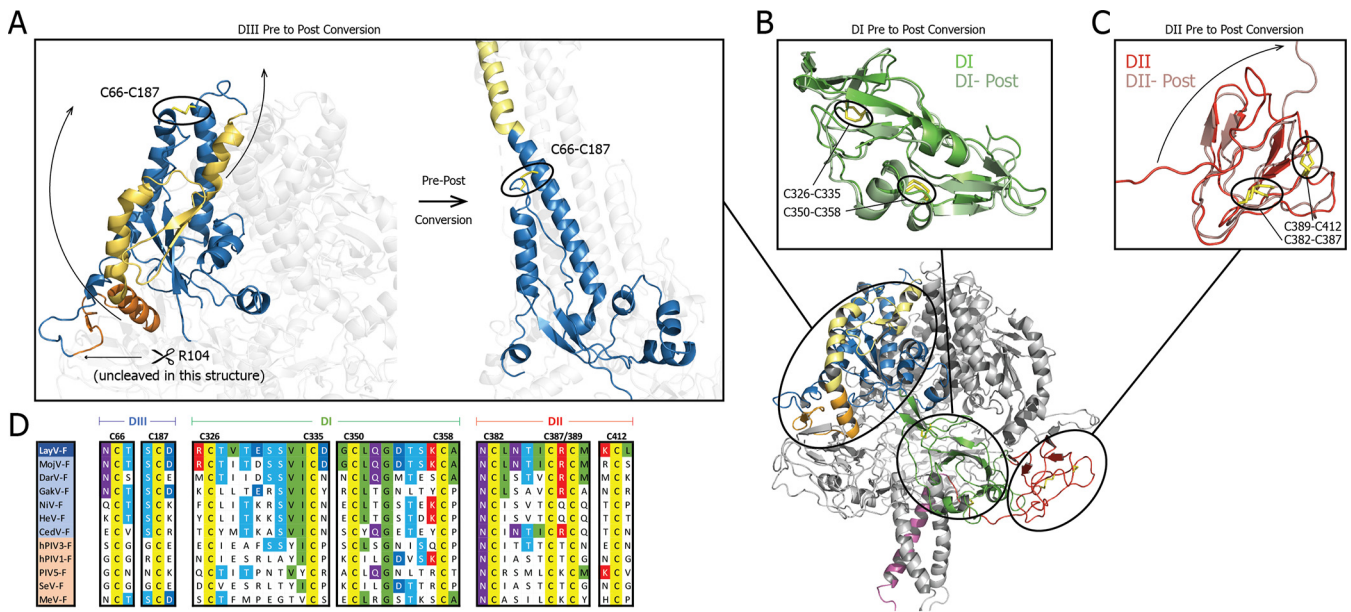
FIG 2 Role of conserved cysteines during conformational conversion. Demonstration of the role of conserved cysteines in each domain in pre- to postfusion conformational changes. (A) Zoomed-in view of the DIII domain, including the fusion peptide (orange) and HRA (yellow), shown for the prefusion (left) and postfusion (right) structures. Color scheme continued from Fig. 1E. The cleavage site at R104 is identified, as well as the disulfide bond formed by C66 and C187 (yellow sticks). This disulfide bond is a hinge point around which the HRA straightens into the central coiled-coil in the postfusion F structure. (B and C) Superimposition of pre- and postfusion conformation domains DI (B) and DII (C). Color scheme continued from Fig. 1E, with the postfusion conformation colored in a lighter shade. Disulfide bonds are shown as yellow sticks and labeled. For DII, the movement of the HRB linker region is indicated by an arrow. (D) Sequence alignment of paramyxovirus fusion proteins in the regions surrounding conserved cysteines, with cysteine residue numbers and domains labeled. Viruses colored blue are from the *Henipavirus* genus and colored tan for other paramyxoviruses. Residues are colored by type per MView standard (51). Blue, alcohol; green, hydrophobic; dark blue, negative charge; red, positive charge; purple, polar; yellow, cysteine.

Despite the drastically different shapes of the pre- and postfusion conformations of LayV-F resulting in a 51.6-Å $C\alpha$ root mean square deviation (RMSD), superimposition of the DI and DII domains demonstrates that these domains remain largely invariant through the pre- to postfusion transition of the F protein (Fig. 2A to C). Both DI and DII domains have two internal pairs of disulfide bonds that help maintain the rigidity of these domains (Fig. 2B to D). DI shows a pre- to postfusion $C\alpha$ RMSD of 2.16 Å, while DII undergoes more total movement, resulting in pre- to postfusion $C\alpha$ RMSD of 16.5 Å with the linker region from S423 to I446 that leads to HRB extending away from the domain as HRB moves to its postfusion location (Fig. 2C). Excluding these residues from the RMSD calculations, DII shifts only 2.3 Å. The difference in conformation of DIII from pre- to postfusion is more dramatic. Based on sequence alignment, the F_1-F_2 cleavage site for LayV-F is expected to be immediately after the highly conserved residue R104 (Fig. S1); however, cleavage did not occur in this construct (Fig. S2C and D). The largest positional shifts during the pre- to postfusion transition occurred in the fusion peptide and HRA, which extend and continue along the path of the apical helix, now forming the central coiled-coil (Fig. 1A). These movements occur around a hinge point in DIII where the apical helix is connected to the rest of DIII by a disulfide bond, again demonstrating the role of the conserved cysteines in providing an anchor for large conformational changes in the F protein (Fig. 2A).

Fusion-triggering mechanism of *Henipavirus* fusion proteins. Insertion of the hydrophobic FP into the host membrane is an essential step that leads to the fusion of the virus and host cell membranes. In the prefusion LayV-F, a substantial portion of the FP is buried within a pocket formed between two LayV-F protomers, requiring the FP to be released from this pocket during the pre- to postfusion conformational transition (Fig. 3). Hydrophobic

FIG 1 Legend (Continued)

different shades of blue (prefusion) and yellow (postfusion) for each protomer. Representative reference-free 2D classes used for the reconstruction are displayed above each map. (C and D) Cartoon representation of atomic models of LayV-F in prefusion (C) and postfusion (D) conformations that were built into the maps shown in panels A and B. In each, one protomer is colored by domain, based on the color scheme in panel E, and the other two protomers are colored gray. (E) Sequence domain key for LayV-F. SS, secretion signal, cleaved prior to purification. DI, DII, and DIII, domains I, II, and III, respectively; FP, fusion peptide; HRA and HRB, heptad repeats A and B, respectively; foldon, trimerization domain; TS, Twin-Strep tag, used for purification with modified streptavidin resin.
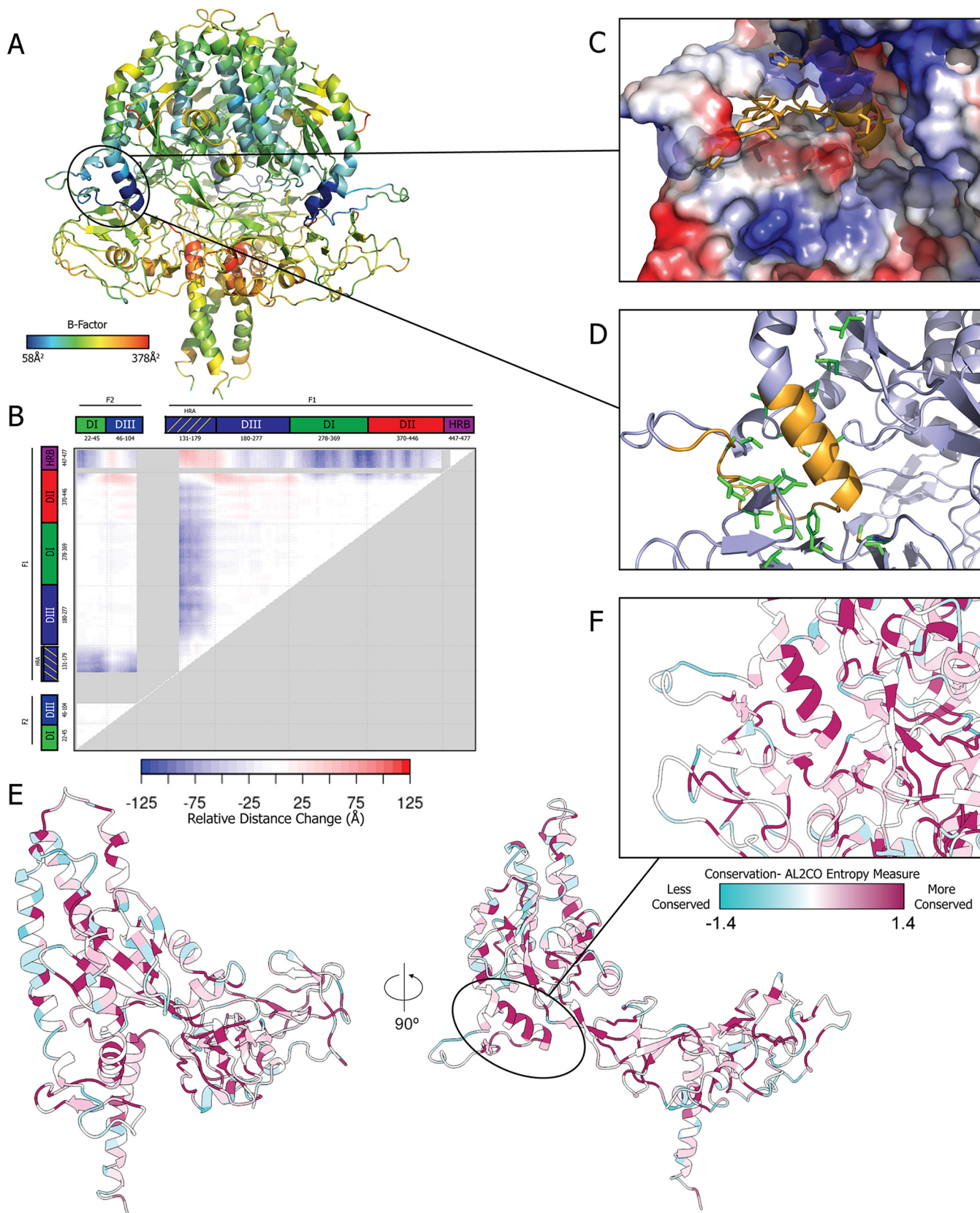
FIG 3 Fusion peptide burial and conservation. (A) Exploration of motion in the pre-F structure through B factor and DDM analysis, with a focus on the features and sequence conservation of the fusion peptide pocket. (A) Structure of the prefusion LayV-F protein shown in the cartoon representation and colored by B factors. (B) Difference distance matrix plot comparing relative residue positions between prefusion and postfusion conformation. Sequence key from Fig. 1E included along each

residues lining the interprotomer pocket into which the FP is buried in the prefusion LayV-F include L51, L89, M92, L93, V96, V216, and I262 from DIII and A108, M110, G112, A114, L115, and G116 from the N-terminal end of the FP upstream of the helical segment from the same protomer, and residues from the adjacent protomer include M292 from DI and P369, F371, A372, L373, G376, V378, I420, L421, and I422 from DII (Fig. 3D).

Consistent with the close packing of the FP within an interprotomer pocket in the prefusion F conformation, the modeled coordinates exhibit the lowest B factors at the FP, while HRB, its DII linker, and the surrounding DI region have the highest B factors in the structure (Fig. 3A). The HRA, HRB, and FP undergo dramatic shifts in their positions during pre-to postfusion conformational change of the LayV-F protein (Fig. 3B). Although the FP is not resolved in the postfusion state, based on its location, it is expected to show a position shift similar to that of HRA. The burial of the prefusion FP and its interactions with the residues lining the interprotomer pocket suggest that the purpose of this pocket is to hold the FP in place to prevent premature conversion to the postfusion form and therefore is the source of metastability of the prefusion LayV-F structure. Consistent with a key role in pre- to postfusion conformational dynamics, the FP and the surrounding pocket are among the most conserved regions in *Henipavirus* fusion proteins (Fig. 3E and F). Release of the FP from this pocket is a requirement for the transition of the F protein from the prefusion to postfusion conformation, and disruption of this pocket may be the mechanism by which the FP is released to undergo these changes.

Structural conservation and antigenic diversity of *Henipavirus* fusion proteins. Despite low overall sequence conservation, the structural similarity of paramyxovirus fusion proteins is striking. Structures have previously been determined for the F proteins of two henipaviruses in the prefusion state, NiV-F and HeV-F (15, 24). Despite having only 38% sequence identity with these viruses, a superimposition of LayV-F with these structures reveals a conserved architecture (Fig. 4A), with Cα RMSDs of 2.64 Å and 3.00 Å for LayV-F to NiV-F and HeV-F, respectively, with NiV-F and HeV-F differing between each other by 0.94 Å. One of the few areas between these species where there is a notable shift is in HRA. In the prefusion conformation, the central helix in HRA is broken by a short, two-stranded β-sheet with a loop that extends to the exterior of the protein. Compared to the homologous HRA loop in NiV and HeV-F, in LayV-F, there is a shift of ~9 Å in the direction of the fusion peptide (Fig. 4B). The cryo-EM reconstruction in this region at an estimated local resolution of ~5Å (Fig. S3) is resolved well enough to allow unambiguous assignment of the main chain for this loop. It is unclear if this shift results in any mechanistic effect on the HRA region, although the loop resides within a site targeted by antibodies, and a shift in its position may alter antigenicity of the F protein (Fig. 4C).

An overlay of all experimentally determined structures of paramyxovirus-targeted antibodies highlights the antigenicity of the HRA loop site and its adjacent regions (Fig. 4C; Fig. S5). Several antibodies target DIII in the prefusion F near the HRA region and likely interfere with pre- to postfusion conversion. In addition to the HRA loop shift described above, LayV-F and other paramyxovirus species show differences in their surface-exposed residues in these regions that could define the unique antigenic properties of the different F proteins. These include a glycosylation site in LayV-F at N279 (Fig. 4D), which is positioned between DI and DIII near several of the previously identified epitopes, specifically of 15F, an HeV-neutralizing antibody, and 5B3, a cross-reactive NiV- and HeV-neutralizing antibody (30).

The sequences of both NiV-F and HeV-F have two plausible glycosylation sites at N64 and N67, both at the apex, though previous studies have established that only N67 is glycosylated (31, 32). The N65 glycosylation position in LayV-F is shifted by 8.2 Å away from the apex residues of HRA. This glycan was particularly visible in the cryo-EM reconstructions of

FIG 3 Legend (Continued)

axis. Gray areas in the bottom right half of the plot are the result of sequences not present in the postfusion model. (C) Hydrophobic fusion peptide pocket in the prefusion state, with fusion peptide depicted as orange cartoon and surface electrostatic view of the pocket. (D) Side chain stick view of the fusion peptide pocket, with hydrophobic residues involved shown with side chains as green sticks. (E) Cartoon representations of a single prefusion-state protomer, colored by sequence conservation across *Henipavirus* fusion proteins. Color scale generated by ChimeraX default AL2CO entropy measure. (F) Zoomed-in view of the fusion peptide pocket, colored by sequence conservation as in E. The fusion peptide pocket is among the most strongly conserved regions of the protein.
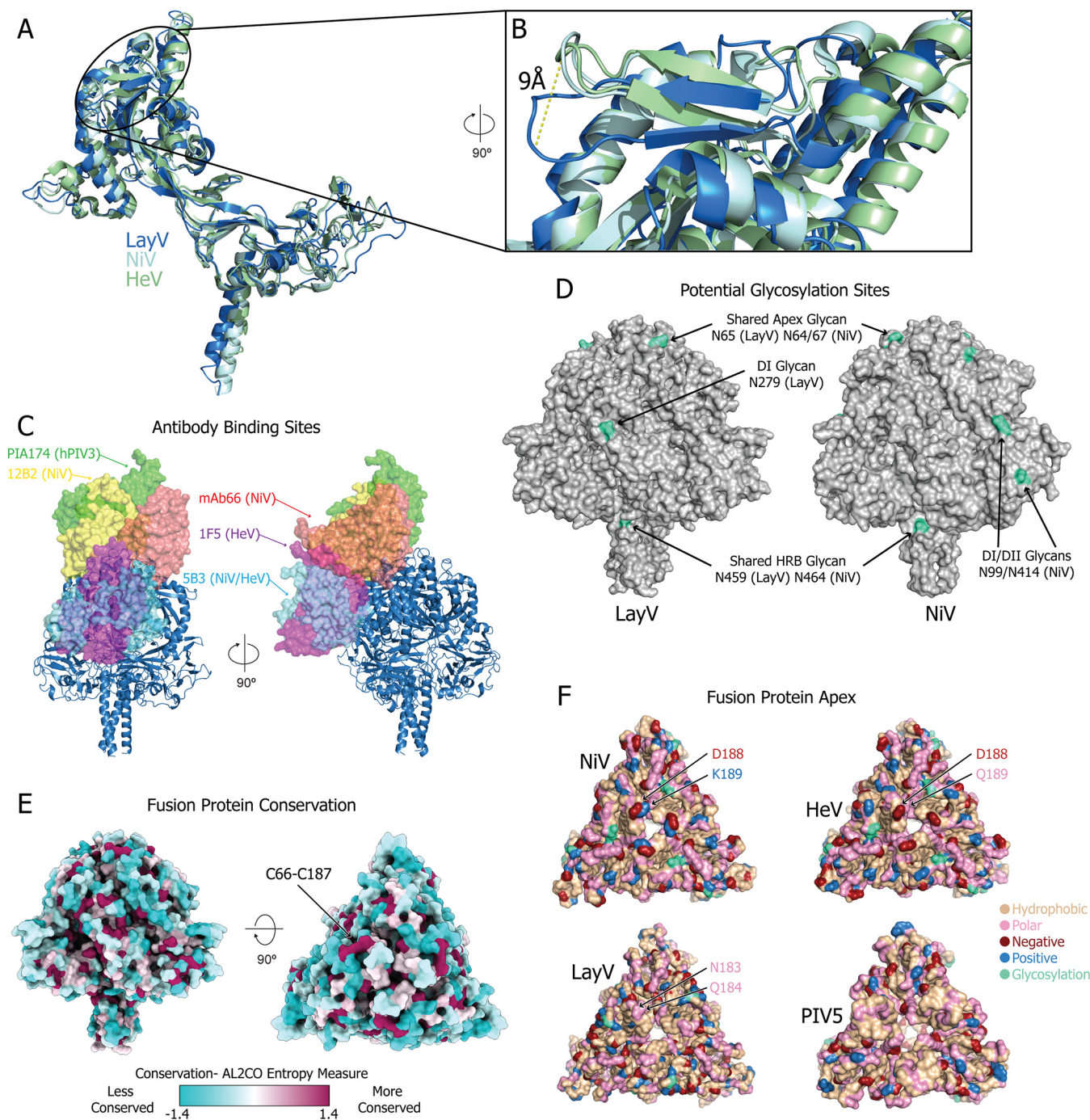
FIG 4 Structure and antigenicity comparison of *Henipavirus* fusion proteins. Comparison of LayV-F structures, surface residue types, and glycosylation patterns of previously determined NiV-F and HeV-F structures, with a focus on important antigenic sites. (A) Superimposition of a single prefusion protomer of LayV-F (blue), NiV-F (cyan), and HeV-F (green) in cartoon representation. PDB accession numbers are 8FEJ for LayV-F, 5EVM for NiV-F, and 5EJB for HeV-F (15, 24). (B) Zoomed-in view of a loop within the folded HRA, one of the few areas of significant structural difference between LayV-F and NiV/HeV-F. (C) Binding site of known paramyxovirus F protein-neutralizing antibodies, labeled by the species targeted. NiV-F trimer from the 12B2-bound structure shown as cartoon and antibody Fabs shown in surface view. Only one Fab per type shown; all except PIA174 bind with 3:1 stoichiometry. PDB accession numbers are 6MJZ for PIA174, 7KI4 for 12B2, 6T3F for mAb66, 7KI6 for 1F5, and 6TYS for 5B3 (25, 30, 52). (D) Surface view of LayV-F and NiV-F, with glycosylation sites (residues meeting the N-X-S/T glycosylation sequence) colored teal. (E) Surface representation of LayV-F colored by sequence conservation across *Henipavirus* fusion proteins. Color scale generated by ChimeraX default AL2CO entropy measure; magenta indicates high conservation, and teal indicates high variability (53). (F) Surface representation of paramyxovirus fusion proteins, showing only main chain atoms, colored by residue type and shown from top-down view. Tan, hydrophobic; pink, polar; red, negative; blue, positive; teal, potential glycosylation. PIV5, PBD accession no. 4GIP (23).

the postfusion conformation before local refinement, where the density at roughly the half-height point of the map corresponds to N65 (Fig. S3, lower right box). Interestingly, sequence alignment reveals that the LayV-F N65 glycosylation site is not homologous to either N64 or N67 of NiV and HeV but, rather, is equivalent to residue 70 (Fig. S1). Viewing the fusion protein colored by sequence conservation further highlights the variability of this region (Fig. 4E). While there are highly conserved residues at discrete points of the surface, namely, the highly conserved disulfide bond near the apex, the surrounding region ranges from moderately conserved to highly variable, especially in surface-accessible regions of DIII and the HRA loop. This variability includes differing residue types between LayV and other henipaviruses, particularly at the apex site. The differences in the prefusion F protein trimer apex are highlighted by a negatively charged residue, D188, in both NiV and HeV, while the LayV-F protein instead has polar residues (N183, Q184) and an overall greater hydrophobic character. This residue arrangement in the prefusion LayV-F trimer apex is more similar to that of the PIV5 prefusion F protein (Fig. 4F). This change in residue type is likely a source of antigenic variability between paramyxovirus F proteins. Consistent with this variability, antibody 12B2, which binds an epitope in prefusion NiV-F that includes the trimer apex (30, 33), did not show binding to LayV-F (Fig. S2F). Therefore, despite similar F protein architecture, antigenic variability within paramyxoviruses is driven by variability of surface residues.

DISCUSSION

The continuing emergence of new paramyxovirus species necessitates heightened focus on a family that includes both some of the world's deadliest pathogens in Nipah virus and the most infectious in measles and mumps. Members specifically of the *Henipavirus* genus have spread to humans through zoonotic transfer. While Nipah and Hendra viruses are spread to humans through bats, new henipaviruses have been detected in a range of species, such as shrews and rats. The role of animal reservoirs in the SARS-CoV-2 pandemic highlights the risk factor that a diverse range of animal hosts can be, further necessitating efforts to develop treatments or vaccines against henipaviruses. Structural determinations of *Henipavirus* glycoproteins serve as a foundation for immunogen or therapeutic design.

Though the structure of LayV-F is strikingly similar to other known *Henipavirus* F structures, key differences in surface characteristics at the apex have implications for pan-henipavirus or pan-paramyxovirus vaccine development. When developing vaccinations for a virus that is quickly mutating, such as SARS-CoV-2, or for a virus with many distinct strains, as observed with henipaviruses, it is important to target relatively invariable sites for immunogen design. Our prefusion LayV-F protein structure helps to demonstrate the particularly variable nature of the apex and DIII in *Henipavirus* F proteins, a trait to be considered when selecting antigenic sites to target for a broad immunogenic response.

In contrast to existing structures of paramyxovirus fusion proteins that were determined in either pre- or postfusion conformation, our study resolves the LayV-F pre- and postfusion structures within the same cryo-EM data set, suggesting that for LayV-F, being in solution at ambient temperatures may allow the proteins to sample enough conformational states such that some will lead to conversion. Though paramyxovirus fusion proteins must be cleaved to enable fusion peptide insertion, prior studies have observed uncleaved fusion proteins assuming a postfusion conformation (34). Our structures reveal a highly stable configuration of the fusion peptide in the prefusion F conformation, buried within an interprotomer pocket, which must be disrupted to transition to the postfusion conformation. These observations suggest that FP configuration is a source of metastability in the prefusion LayV-F protein, where a shift in the position of the FP or the residues surrounding it in the interprotomer pocket too far from its prefusion configuration may lead to irreversible conversion to the postfusion form. This, together with the biochemical properties of the FP burial pocket, suggests tight control of FP positioning is an important part of prefusion metastability. While the use of an ectodomain construct without stabilizing mutations did allow for flexibility that hindered high-resolution reconstruction, this made the relative lack of flexibility in the FP region more readily apparent, indicating a unique arrangement of FP
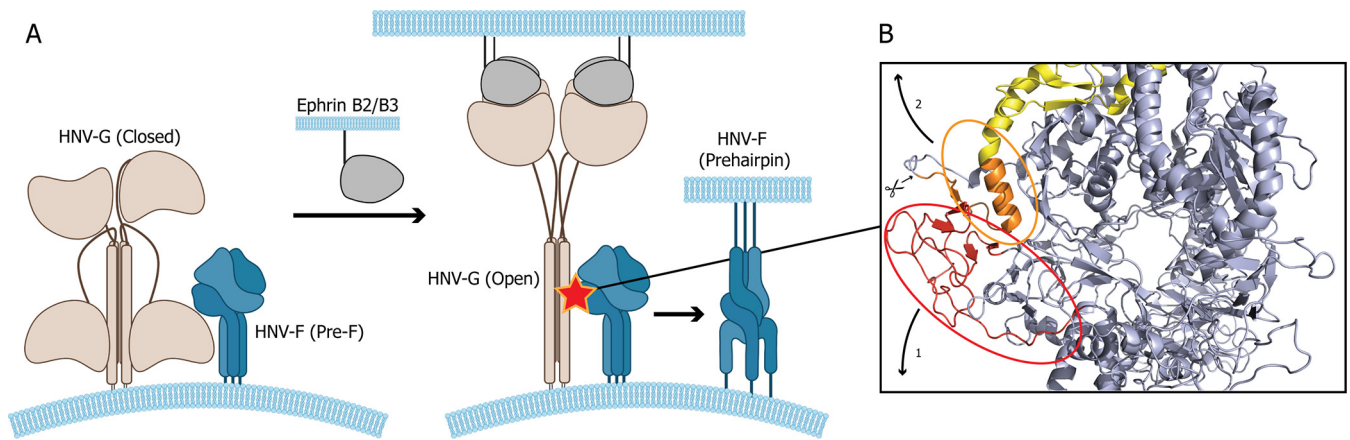
FIG 5 Fusion-triggering hypothesis for paramyxoviruses. Proposed mechanism of *Henipavirus* fusion triggering based on new data and previous knowledge. (A) Existing model of *Henipavirus* (HNV) fusion protein triggering based on Liu et al. (36). HNV-G, brown, shown in a two-receptor binding domain down "closed" state, bound to HNV-F in prefusion conformation. Exposure to ephrin B2 and B3 receptors induces opening of HNV-G, triggering conversion of HNV-F from prefusion to the prehairpin state. The triggering interaction is labeled with a star. (B) Hypothesized structural basis for the G-F interaction shown in panel A, wherein a two-step mechanism involving disruption of the fusion peptide burial pocket through the action of the HNV-G stalk on DII frees the fusion peptide, allowing conformational conversion. The figure was made using resources from BioRender.

conformation in paramyxoviruses compared to other fusion proteins (see Fig. S4 and Supplemental Note 1 in the supplemental material).

An elusive question regarding paramyxovirus fusion is how the fusion process is first initiated. For the many virus families that utilize a fusion protein, the metastable prefusion state is maintained prior to a triggering event that initiates conformational changes. In many cases, this process involves cleavage and removal of entire domains of the fusion protein, such as with the removal of the S1 subunit from the SARS-CoV-2 spike protein prior to fusion. The paramyxovirus fusion proteins, however, have no such attachment subunit to remove. Instead, paramyxoviruses utilize a separate attachment protein, which is thought to pass on a triggering signal to the fusion protein after receptor binding (13, 14) (Fig. 5A). For some paramyxovirus species, the attachment and fusion proteins have been shown to form complexes prior to receptor engagement (13) (Fig. 5A). Structural characterization of such complexes had been elusive, but recently, a structure of the human parainfluenza virus (hPIV3) attachment-fusion (HN-F) complex has been determined by cryo-electron tomography (35). One of the receptor-binding domains of HN is seen to bind at the apex of F, presumably stabilizing the prefusion conformation of F. While this might suggest a mechanism where the attachment protein functions as a clamp on the fusion protein, maintaining the prefusion state until receptor binding, studies assaying fusion competency have demonstrated that the fusion protein alone is not sufficient for virus and host cell fusion, which reinforces that paramyxovirus F proteins achieve inherent metastability that does not fully depend on an external clamp and indicates that fusion triggering involves a more complex mechanism of interaction between the two proteins (36, 37).

The structural similarities seen between the paramyxovirus fusion proteins of different species also extend to the receptor-binding head domains of paramyxovirus attachment proteins. In the hPIV3 HN-F structure, a loop from the HN head that inserts into a cavity formed at the trimer interface at the apex of F, which is noted to be one such area of structural conservation between different paramyxovirus genera, possibly revealing a conserved mode of complex formation (35). However, while the *Henipavirus* F proteins generally are generally glycosylated at their apexes, albeit not at a strictly conserved residue, hPIV3 does not have a canonical N-X-S/T glycosylation motif at its apex, and previous structures have not identified apex glycosylation for hPIV3F. The presence of glycans in henipaviruses could add steric hindrance that may change the nature of this complex formation within this genus. It should be noted, however, that while hPIV3 has no canonical glycosylation motif at the apex, it does contain an N-X-C motif at residue 61 in the apex, which is a less frequently glycosylated sequence (38).

The fusion peptide in the prefusion LayV-F protein is in a configuration that is conserved among paramyxoviruses and distinct from other class I fusion proteins (Fig. S4; Supplemental Note 1). It is not yet known which residues are involved in the interaction between the attachment and fusion proteins, but the critical role of the FP pocket created at the DII-DIII interface suggests that DII could be the site of the interaction. The triggering signal may be transferred by way of the attachment protein repositioning DII such that the fusion peptide is released from the pocket, irreversibly extending toward the apex (Fig. 5B). This mechanism would be consistent with previous paramyxovirus studies that suggested an attachment protein-binding role for DII (39, 40). Further supporting this hypothesis is the likelihood that the FP in the prefusion conformation is in a high-energy state due to the kink in the helix comprised of the FP from T119 through HRA up to N148. Such a helix shape is often brought about by the presence of a proline at the kink, introducing bond-angle limitations that force this shape into the helix (41). However, in the helix containing the FP, no proline is present. The bent shape could be induced by the FP being buried within and locked into the hydrophobic FP pocket. When disrupted, the position of the FP would therefore move rapidly as the tension in the helix is resolved. Though it could be hypothesized that cleavage of the FP is the trigger that allows for rearrangement, our study, in line with others, has established that cleavage is not required for conformational conversion in paramyxovirus fusion proteins.

The existence of a high-energy-state FP helix, held in place by an interprotomer DII, which is then disrupted by the action of an attachment protein, offers a hypothesis for how *Henipavirus* attachment proteins activate their conjugate fusion proteins and the basis for how paramyxovirus fusion proteins maintain their metastability in the prefusion state. Additional experiments, including biochemical studies assaying the effect of mutations in the FP-DII interface designed to stabilize or destabilize the interaction, will be needed to further explore this hypothesized mechanism of *Henipavirus* F metastability. Furthermore, while this study adds to the myriad of structural information on paramyxovirus F proteins, the breadth of information on paramyxovirus attachment protein structure remains comparatively lesser. Given the high variability in the stalk and neck domains of attachment proteins that may play a role in enabling complex formation and fusion activation, expanded structural information may be needed for effective experimental design that biochemically validates the nature of the attachment-fusion interaction.

MATERIALS AND METHODS

Plasmids. Gene synthesis for all plasmids generated by this study was performed and the sequence confirmed by GeneImmune Biotechnology (Rockville, MD). The fusion protein ectodomain constructs included F protein residues 1 to 438 (GenPept accession no. UUV47205), a C-terminal T4 fibritin trimerization motif (foldon), a C-terminal HRV3C protease cleavage site, a Twin-Strep tag, and an $8 \times$ His tag. The ectodomain was cloned into the mammalian expression vector pαH. Synthetic heavy and light chain variable-domain genes for Fabs were cloned into a modified pVRC8400 expression vector as previously described (5, 24, 25). Antibody-variable regions for both heavy and light chain replaced the variable regions from the VRC01 antibody plasmid (42), with the interleukin 2 (IL-2) secretion signal and human kappa constant domain being used for light chain plasmids. All plasmids have been deposited to Addgene (https://www.addgene.org) under the codes 200390, 200391, 200392, 200398, and 200399.

Cell culture and protein expression. For F ectodomains, Gibco FreeStyle 293-F cells (embryonal, human kidney) were maintained at 37℃ and 9% CO_2 in a 75% humidified atmosphere in FreeStyle 293 expression medium (Gibco). The plasmid was transiently transfected using Turbo293 (Speed BioSystems) and incubated at 37℃, 9% CO_2, and 75% humidity with agitation at 120 rpm for 6 days. On the day following transfection, HyClone CDM4HEK293 medium (Cytiva, MA) was added to the cells. For antibodies, Gibco Expi293F cells (embryonal, human kidney) were maintained at 37℃ and 9% CO_2 in a 75% humidified atmosphere in Expi293 expression medium (Gibco). The plasmid was transiently transfected using ExpiFectamine 293 (Gibco) and incubated at 37℃, 9% CO_2, and 75% humidity with agitation at 120 rpm for 6 days. On the day following transfection, ExpiFectamine 293 enhancers (Gibco) were added to the cells.

Protein purification. On the 6th day post-transfection, the fusion protein ectodomains were harvested from the concentrated supernatant and purified using Strep-Tactin resin (IBA Lifesciences) and size exclusion chromatography (SEC) using a Superose 6 Increase 10/300 GL column (Cytiva, MA) equilibrated in phosphate-buffered saline (PBS) buffer (Thermo Scientific; 137 mM NaCl, 2.7 mM KCl, pH 7.4, 10 mM phosphate buffer, and 1.8 mM potassium phosphate monobasic). Antibodies were purified using protein A affinity (Thermo Scientific) and SEC using a Superose 6 Increase 10/300 GL column equilibrated in PBS buffer. All steps of the purification were performed at room temperature and in a single day. Protein quality was assessed by

SDS-PAGE using NuPAGE 4 to 12% (Invitrogen, CA). The purified proteins were flash frozen and stored at −80°C in single-use aliquots. Each aliquot was thawed by a 5-min incubation at 37°C before use.

Cryo-EM. The purified ectodomain was diluted to a concentration of 1.5 mg/mL in PBS (described above) 0.0085 mM n-dodecyl β-D-maltoside (DDM) and 0.38% glycerol added. A 2.2-μL drop of protein was deposited on a Quantifoil R1.2/1.3 grid (Electron Microscopy Sciences, PA) that had been glow discharged for 10 s using a Pelco easiGlow glow discharge cleaning system. After a 30-s incubation in >95% humidity, excess protein was blotted away for 2.5 s before being plunged frozen into liquid ethane using a Leica EM GP2 plunge freezer (Leica Microsystems). Frozen grids were imaged using a Titan Krios (Thermo Fisher) equipped with a K3 detector (Gatan). Movie frame alignment was carried out using Unblur (43). cryoSPARC (44) software was used for data processing. Phenix (45), PyMOL (Schrödinger, LLC), ChimeraX (46), and ISOLDE (47) were used for model building and refinement. Phenix was first used to fit the initial models into maps. ISOLDE was used to manually adjust residues to address rotamer and Ramachandran outliers. Phenix was again used to perform real-space refinement and energy minimization of side chain positions and to set B factors during an ADP-only real-space refinement. The resolution of both structures did not allow for experimental determination of side chain positions; therefore, energy minimization followed by optimization of rotamer positions described above is the basis for side chains in the model.

SDS-PAGE. 1, 3, or 8 μg of sample was prepared with Laemmli sample buffer (Bio-Rad), PBS buffer, and with or without 300 mM dichlorodiphenyltrichloroethane (DTT; reduced/nonreduced). Samples were loaded to NuPAGE 4 to 12% Bis-Tris gels (Invitrogen) and ran at 175 V with morpholineethanesulfonic acid-SDS (MES-SDS) running buffer until complete. Samples were stained with Coomassie blue (Novex) for 30 min before water destaining and imaging.

Differential scanning fluorimetry. The DSF assay was performed using Tycho NT.6 (NanoTemper Technologies). Spike ectodomains were diluted to approximately 0.15 mg/mL. Intrinsic fluorescence was measured at 330 nm and 350 nm while the sample was heated from 35 to 95°C at a rate of 30°C/min. The ratio of fluorescence (350/330 nm) and inflection temperature (T_i) was calculated by the Tycho NT.6 apparatus.

DDMs. Difference distance matrix (DDM) plots were generated using the Bio3D package (48) implemented in R (49; http://www.R-project.org/).

BLI. Antibody binding to *Henipavirus* F proteins was assessed using biolayer interferometry (BLI) on an Octet Red 384 (Sartorius, formerly ForteBio) with ForteBio kinetics buffer. All binding assays were performed at 30°C. Antibodies were immobilized on anti-human Fc capture tips (ForteBio), loaded at 20 μg/mL for 300 s. F proteins were used as analytes at 100 nM, with an association time of 480 s and dissociation time of 600 s. Sensorgram data were reference subtracted and analyzed using the Octet Analysis Studio software (Sartorius), with a reference tip for each immobilized antibody and reference sample for each analyte.

Sequence alignment. Paramyxovirus F sequences were aligned with Clustal Omega tool (50). Output alignment was colored and assigned consensus residue types by MView (51). Sequences were obtained from either UniProt or GenBank. UniProt accession numbers used were Q9IH63 for NiV-F, O89342 for HeV-F, P06828 for hPIV3-F, P04849 for PIV5-F, Q786F3 for MeV-F (Ichinose-B95a Strain), W8SKT3 for MojV-F, J7GX38 for Cedarvirus F (CedV-F), P12605 for hPIV1-F, P26628 for NDV-F (Texas strain), and P04855 for SeV-F (Z strain). GenPept accession numbers used were UUV47205 for LayV-F, QYO90524 for GakV-F, and QYO90531 for DarV-F.

Data availability. Cryo-EM reconstructions and atomic models generated during this study are available at PDB and EMBD (https://www.rcsb.org and http://emsearch.rutgers.edu, respectively) under the PDB accession numbers 8FEJ and 8FEL and EMDB accession numbers EMD-29029 and EMD-29032.

SUPPLEMENTAL MATERIAL

Supplemental material is available online only.
SUPPLEMENTAL FILE 1, PDF file, 10.7 MB.
SUPPLEMENTAL FILE 2, DOCX file, 0.02 MB.

ACKNOWLEDGMENTS

REFERENCES

1. Zhang X-A, Li H, Jiang F-C, Zhu F, Zhang Y-F, Chen J-J, Tan C-W, Anderson DE, Fan H, Dong L-Y, Li C, Zhang P-H, Li Y, Ding H, Fang L-Q, Wang L-F, Liu W. 2022. A zoonotic henipavirus in febrile patients in China. N Engl J Med 387:470–472. https://doi.org/10.1056/NEJMc2202705.

2. Wu Z, Yang L, Yang F, Ren X, Jiang J, Dong J, Sun L, Zhu Y, Zhou H, Jin Q. 2014. Novel Henipa-like virus, Mojiang paramyxovirus, in rats, China, 2012. Emerg Infect Dis 20:1064–1066. https://doi.org/10.3201/eid2006.131022.

3. Lee S-H, Kim K, Kim J, No JS, Park K, Budhathoki S, Lee SH, Lee J, Cho SH, Cho S, Lee G-Y, Hwang J, Kim H-C, Klein TA, Uhm C-S, Kim W-K, Song J-W. 2021. Discovery and genetic characterization of novel paramyxoviruses related to the genus henipavirus in Crocidura species in the Republic of Korea. Viruses 13:2020. https://doi.org/10.3390/v13102020.

4. Field H, Young P, Yob JM, Mills J, Hall L, Mackenzie J. 2001. The natural history of Hendra and Nipah viruses. Microbes Infect 3:307–314. https://doi.org/10.1016/s1286-4579(01)01384-3.

5. Rima B, Balkema-Buschmann A, Dundon WG, Duprex P, Easton A, Fouchier R, Kurath G, Lamb R, Lee B, Rota P, Wang L, Ictv Report Consortium. 2019. ICTV virus taxonomy profile: Paramyxoviridae. J Gen Virol 100:1593–1594. https://doi.org/10.1099/jgv.0.001328.

6. World Health Organization. Prioritizing diseases for research and development in emergency contexts. https://www.who.int/activities/prioritizing-diseases-for-research-and-development-in-emergency-contexts. Retrieved 28 February 2023.

7. Aguilar HC, Iorio RM. 2012. Henipavirus membrane fusion and viral entry, p 79–94. In Lee B, Rota PA (ed), Henipavirus: ecology, molecular virology, and pathogenesis. Springer, Berlin, Heidelberg, Germany.

8. Negrete OA, Levroney EL, Aguilar HC, Bertolotti-Ciarlet A, Nazarian R, Tajyar S, Lee B. 2005. EphrinB2 is the entry receptor for Nipah virus, an emergent deadly paramyxovirus. Nature 436:401–405. https://doi.org/10.1038/nature03838.

9. Xu K, Rajashankar KR, Chan Y-P, Himanen JP, Broder CC, Nikolov DB. 2008. Host cell recognition by the henipaviruses: crystal structures of the Nipah G attachment glycoprotein and its complex with ephrin-B3. Proc Natl Acad Sci U S A 105:9953–9958. https://doi.org/10.1073/pnas.0804797105.

10. White JM, Delos SE, Brecher M, Schornberg K. 2008. Structures and mechanisms of viral membrane fusion proteins: multiple variations on a common theme. Crit Rev Biochem Mol Biol 43:189–219. https://doi.org/10.1080/10409230802058320.

11. Lamb RA, Jardetzky TS. 2007. Structural basis of viral invasion: lessons from paramyxovirus F. Curr Opin Struct Biol 17:427–436. https://doi.org/10.1016/j.sbi.2007.08.016.

12. Pager CT, Dutch RE. 2005. Cathepsin L is involved in proteolytic processing of the Hendra virus fusion protein. J Virol 79:12714–12720. https://doi.org/10.1128/JVI.79.20.12714-12720.2005.

13. Bose S, Jardetzky TS, Lamb RA. 2015. Timing is everything: fine-tuned molecular machines orchestrate paramyxovirus entry. Virology 479–480:518–531. https://doi.org/10.1016/j.virol.2015.02.037.

14. Iorio RM, Melanson VR, Mahon PJ. 2009. Glycoprotein interactions in paramyxovirus fusion. Future Virol 4:335–351. https://doi.org/10.2217/fvl.09.17.

15. Xu K, Chan Y-P, Bradel-Tretheway B, Akyol-Ataman Z, Zhu Y, Dutta S, Yan L, Feng Y, Wang L-F, Skiniotis G, Lee B, Zhou ZH, Broder CC, Aguilar HC, Nikolov DB. 2015. Crystal structure of the pre-fusion Nipah virus fusion glycoprotein reveals a novel hexamer-of-trimers assembly. PLoS Pathog 11:e1005322. https://doi.org/10.1371/journal.ppat.1005322.

16. Loomis RJ, Stewart-Jones GBE, Tsybovsky Y, Caringal RT, Morabito KM, McLellan JS, Chamberlain AL, Nugent ST, Hutchinson GB, Kueltzo LA, Mascola JR, Graham BS. 2020. Structure-based design of Nipah virus vaccines: a generalizable approach to paramyxovirus immunogen development. Front Immunol 11:842. https://doi.org/10.3389/fimmu.2020.00842.

17. Hsieh C-L, Goldsmith JA, Schaub JM, DiVenere AM, Kuo H-C, Javanmardi K, Le KC, Wrapp D, Lee AG, Liu Y, Chou C-W, Byrne PO, Hjorth CK, Johnson NV, Ludes-Meyers J, Nguyen AW, Park J, Wang N, Amengor D, Lavinder JJ, Ippolito GC, Maynard JA, Finkelstein IJ, McLellan JS. 2020. Structure-based design of prefusion-stabilized SARS-CoV-2 spikes. Science 369:1501–1505. https://doi.org/10.1126/science.abd0826.

18. Wrapp D, Wang N, Corbett KS, Goldsmith JA, Hsieh C-L, Abiona O, Graham BS, McLellan JS. 2020. Cryo-EM structure of the 2019-nCoV spike in the prefusion conformation. Science 367:1260–1263. https://doi.org/10.1126/science.abb2507.

19. Do Kwon Y, Pancera M, Acharya P, Georgiev IS, Crooks ET, Gorman J, Joyce MG, Guttman M, Ma X, Narpala S, Soto C, Terry DS, Yang Y, Zhou T, Ahlsen G, Bailer RT, Chambers M, Chuang G-Y, Doria-Rose NA, Druz A, Hallen MA, Harned A, Kirys T, Louder MK, O'Dell S, Ofek G, Osawa K, Prabhakaran M, Sastry M, Stewart-Jones GBE, Stuckey J, Thomas PV, Tittley T, Williams C, Zhang B, Zhao H, Zhou Z, Donald BR, Lee LK, Zolla-Pazner S, Baxa U, Schön A, Freire E, Shapiro L, Lee KK, Arthos J, Munro JB, Blanchard SC, Mothes W, Binley JM, et al. 2015. Crystal structure, conformational fixation and entry-related interactions of mature ligand-free HIV-1 Env. Nat Struct Mol Biol 22:522–531. https://doi.org/10.1038/nsmb.3051.

20. Rawi R, Rutten L, Lai Y-T, Olia AS, Blokland S, Juraszek J, Shen C-H, Tsybovsky Y, Verardi R, Yang Y, Zhang B, Zhou T, Chuang G-Y, Kwong PD, Langedijk JPM. 2020. Automated design by structure-based stabilization and consensus repair to achieve prefusion-closed envelope trimers in a wide variety of HIV strains. Cell Rep 33:108432. https://doi.org/10.1016/j.celrep.2020.108432.

21. Tan YZ, Baldwin PR, Davis JH, Williamson JR, Potter CS, Carragher B, Lyumkis D. 2017. Addressing preferred specimen orientation in single-particle cryo-EM through tilting. Nat Methods 14:793–796. https://doi.org/10.1038/nmeth.4347.

22. Hashiguchi T, Fukuda Y, Matsuoka R, Kuroda D, Kubota M, Shirogane Y, Watanabe S, Tsumoto K, Kohda D, Plemper RK, Yanagi Y. 2018. Structures of the prefusion form of measles virus fusion protein in complex with inhibitors. Proc Natl Acad Sci U S A 115:2496–2501. https://doi.org/10.1073/pnas.1718957115.

23. Welch BD, Liu Y, Kors CA, Leser GP, Jardetzky TS, Lamb RA. 2012. Structure of the cleavage-activated prefusion form of the parainfluenza virus 5 fusion protein. Proc Natl Acad Sci U S A 109:16672–16677. https://doi.org/10.1073/pnas.1213802109.

24. Wong JJW, Paterson RG, Lamb RA, Jardetzky TS. 2016. Structure and stabilization of the Hendra virus F glycoprotein in its prefusion form. Proc Natl Acad Sci U S A 113:1056–1061. https://doi.org/10.1073/pnas.1523303113.

25. Stewart-Jones GBE, Chuang G-Y, Xu K, Zhou T, Acharya P, Tsybovsky Y, Ou L, Zhang B, Fernandez-Rodriguez B, Gilardi V, Silacci-Fregni C, Beltramello M, Baxa U, Druz A, Kong W-P, Thomas PV, Yang Y, Foulds KE, Todd J-P, Wei H, Salazar AM, Scorpio DG, Carragher B, Potter CS, Corti D, Mascola JR, Lanzavecchia A, Kwong PD. 2018. Structure-based design of a quadrivalent fusion glycoprotein vaccine for human parainfluenza virus types 1–4. Proc Natl Acad Sci U S A 115:12265–12270. https://doi.org/10.1073/pnas.1811980115.

26. Yin HS, Wen X, Paterson RG, Lamb RA, Jardetzky TS. 2006. Structure of the parainfluenza virus 5 F protein in its metastable, prefusion conformation. Nature 439:38–44. https://doi.org/10.1038/nature04322.

27. Murray K, Selleck P, Hooper P, Hyatt A, Gould A, Gleeson L, Westbury H, Hiley L, Selvey L, Rodwell B, Ketterer P. 1995. A morbillivirus that caused fatal disease in horses and humans. Science 268:94–97. https://doi.org/10.1126/science.7701348.

28. Madera S, Kistler A, Ranaivoson HC, Ahyong V, Andrianiaina A, Andry S, Raharinosy V, Randriambolamanantsoa TH, Ravelomanantsoa NAF, Tato CM, DeRisi JL, Aguilar HC, Lacoste V, Dussart P, Heraud J-M, Brook CE. 2022. Discovery and genomic characterization of a novel henipavirus, Angavokely virus, from fruit bats in Madagascar. J Virol 96:e00921-22. https://doi.org/10.1128/jvi.00921-22.

29. Hernández LHA, da Paz TYB, Silva S, Silva F, Barros B, Nunes BTD, Casseb LMN, Medeiros DBA, Vasconcelos P, Cruz ACR. 2022. First genomic evidence of a Henipa-like virus in Brazil. Viruses 14:2167. https://doi.org/10.3390/v14102167.

30. Dang HV, Cross RW, Borisevich V, Bornholdt ZA, West BR, Chan Y-P, Mire CE, Da Silva SC, Dimitrov AS, Yan L, Amaya M, Navaratnarajah CK, Zeitlin L, Geisbert TW, Broder CC, Veesler D. 2021. Broadly neutralizing antibody cocktails targeting Nipah virus and Hendra virus fusion glycoproteins. Nat Struct Mol Biol 28:426–434. https://doi.org/10.1038/s41594-021-00584-8.

31. Aguilar HC, Matreyek KA, Filone CM, Hashimi ST, Levroney EL, Negrete OA, Bertolotti-Ciarlet A, Choi DY, McHardy I, Fulcher JA, Su SV, Wolf MC, Kohatsu L, Baum LG, Lee B. 2006. N-glycans on Nipah virus fusion protein protect against neutralization but reduce membrane fusion and viral entry. J Virol 80:4878–4889. https://doi.org/10.1128/JVI.80.10.4878-4889.2006.

32. Carter JR, Pager CT, Fowler SD, Dutch RE. 2005. Role of N-linked glycosylation of the Hendra virus fusion protein. J Virol 79:7922–7925. https://doi.org/10.1128/JVI.79.12.7922-7925.2005.

33. Dang HV, Chan Y-P, Park Y-J, Snijder J, Da Silva SC, Vu B, Yan L, Feng Y-R, Rockx B, Geisbert TW, Mire CE, Broder CC, Veesler D. 2019. An antibody against the F glycoprotein inhibits Nipah and Hendra virus infections. Nat Struct Mol Biol 26:980–987. https://doi.org/10.1038/s41594-019-0308-9.

34. Yin H-S, Paterson RG, Wen X, Lamb RA, Jardetzky TS. 2005. Structure of the uncleaved ectodomain of the paramyxovirus (hPIV3) fusion protein. Proc Natl Acad Sci U S A 102:9288–9293. https://doi.org/10.1073/pnas.0503989102.

35. Marcink TC, Zipursky G, Cheng W, Stearns K, Stenglein S, Golub K, Cohen F, Bovier F, Pfalmer D, Greninger AL, Porotto M, Des Georges A, Moscona A. 2023. Subnanometer structure of an enveloped virus fusion complex on viral surface reveals new entry mechanisms. Sci Adv 9:eade2727. https://doi.org/10.1126/sciadv.ade2727.

36. Liu Q, Stone JA, Bradel-Tretheway B, Dabundo J, Benavides Montano JA, Santos-Montanez J, Biering SB, Nicola AV, Iorio RM, Lu X, Aguilar HC. 2013. Unraveling a three-step spatiotemporal mechanism of triggering of receptor-induced Nipah virus fusion and cell entry. PLoS Pathog 9:e1003770. https://doi.org/10.1371/journal.ppat.1003770.

37. Yeo YY, Buchholz DW, Gamble A, Jager M, Aguilar HC. 2021. Headless henipaviral receptor binding glycoproteins reveal fusion modulation by the head/stalk interface and post-receptor binding contributions of the head domain. J Virol 95:e00666-21. https://doi.org/10.1128/JVI.00666-21.

38. Lowenthal MS, Davis KS, Formolo T, Kilpatrick LE, Phinney KW. 2016. Identification of novel N-glycosylation sites at noncanonical protein consensus motifs. J Proteome Res 15:2087–2101. https://doi.org/10.1021/acs.jproteome.5b00733.

39. Bose S, Heath CM, Shah PA, Alayyoubi M, Jardetzky TS, Lamb RA. 2013. Mutations in the parainfluenza virus 5 fusion protein reveal domains important for fusion triggering and metastability. J Virol 87:13520–13531. https://doi.org/10.1128/JVI.02123-13.

40. Poor TA, Jones LM, Sood A, Leser GP, Plasencia MD, Rempel DL, Jardetzky TS, Woods RJ, Gross ML, Lamb RA. 2014. Probing the paramyxovirus fusion (F) protein-refolding event from pre- to postfusion by oxidative footprinting. Proc Natl Acad Sci U S A 111:E2596–E2605. https://doi.org/10.1073/pnas.1408983111.

41. Wilman HR, Shi J, Deane CM. 2014. Helix kinks are equally prevalent in soluble and membrane proteins. Proteins 82:1960–1970. https://doi.org/10.1002/prot.24550.

42. McCarthy KR, Lee J, Watanabe A, Kuraoka M, Robinson-McCarthy LR, Georgiou G, Kelsoe G, Harrison SC. 2021. A prevalent focused human antibody response to the influenza virus hemagglutinin head interface. mBio 12:e01144-21. https://doi.org/10.1128/mBio.01144-21.

43. Grant T, Grigorieff N. 2015. Measuring the optimal exposure for single particle cryo-EM using a 2.6 Å reconstruction of rotavirus VP6. Elife 4:e06980. https://doi.org/10.7554/eLife.06980.

44. Punjani A, Rubinstein JL, Fleet DJ, Brubaker MA. 2017. cryoSPARC: algorithms for rapid unsupervised cryo-EM structure determination. Nat Methods 14:290–296. https://doi.org/10.1038/nmeth.4169.

45. Liebschner D, Afonine PV, Baker ML, Bunkoczi G, Chen VB, Croll TI, Hintze B, Hung L-W, Jain S, McCoy AJ, Moriarty NW, Oeffner RD, Poon BK, Prisant MG, Read RJ, Richardson JS, Richardson DC, Sammito MD, Sobolev OV, Stockwell DH, Terwilliger TC, Urzhumtsev AG, Videau LL, Williams CJ, Adams PD. 2019. Macromolecular structure determination using X-rays, neutrons and electrons: recent developments in Phenix. Acta Crystallogr D Struct Biol 75:861–877. https://doi.org/10.1107/S2059798319011471.

46. Pettersen EF, Goddard TD, Huang CC, Meng EC, Couch GS, Croll TI, Morris JH, Ferrin TE. 2021. UCSF ChimeraX: structure visualization for researchers, educators, and developers. Protein Sci 30:70–82. https://doi.org/10.1002/pro.3943.

47. Croll T. 2018. ISOLDE: a physically realistic environment for model building into low-resolution electron-density maps. Acta Crystallogr D Struct Biol 74:519–530. https://doi.org/10.1107/S2059798318002425.

48. Grant BJ, Skjærven L, Yao X-Q. 2021. The Bio3D packages for structural bioinformatics. Protein Science 30:20–30. https://doi.org/10.1002/pro.3923.

49. R Core Team. 2018. R: A language and environment for statistical computing. R Foundation for Statistical Computing, Vienna, Austria.

50. Madeira F, Pearce M, Tivey ARN, Basutkar P, Lee J, Edbali O, Madhusoodanan N, Kolesnikov A, Lopez R. 2022. Search and sequence analysis tools services from EMBL-EBI in 2022. Nucleic Acids Res 50:W276–W279. https://doi.org/10.1093/nar/gkac240.

51. Brown NP, Leroy C, Sander C. 1998. MView: a web-compatible database search or multiple alignment viewer. Bioinformatics 14:380–381. https://doi.org/10.1093/bioinformatics/14.4.380.

52. Avanzato VA, Oguntuyo KY, Escalera-Zamudio M, Gutierrez B, Golden M, Kosakovsky Pond SL, Pryce R, Walter TS, Seow J, Doores KJ, Pybus OG, Munster VJ, Lee B, Bowden TA. 2019. A structural basis for antibody-mediated neutralization of Nipah virus reveals a site of vulnerability at the fusion glycoprotein apex. Proc Natl Acad Sci U S A 116:25057–25067. https://doi.org/10.1073/pnas.1912503116.

53. Pei J, Grishin NV. 2001. AL2CO: calculation of positional conservation in a protein sequence alignment. Bioinformatics 17:700–712. https://doi.org/10.1093/bioinformatics/17.8.700.